Research paper

Centrifugal shaking experiments and FEM analytical investigation on masonry block reinforcement of small earth dams

Bohan Wang[1], Yoshiyuki Mohri[2], Hidekazu Tagashira[3], Akira Izumi[4], Tadatsugu Tanaka[5]

Abstract: In this research, a series of centrifuge model tests and dynamic response analyses were conducted to elucidate the impact of a composite structure comprised of a reinforced earth-pressure-resistant technique, using both masonry blocks and the reinforced earth method, which was installed at the slope toe end of an aged reservoir. The purpose of the study was to evaluate the seismic response of the embankment. The experimental tests included shaking table tests that were performed on an unreinforced embankment as well as a masonry block reinforced embankment, both in a water storage condition. The dynamic behavior of the embankment, as well as the propagation of slip failure, were compared and verified. Through the use of elasto-plastic dynamic response analysis, using the finite element method, the location of the slip surface, the settlement of the embankment and the dynamic response characteristics, as obtained experimentally, were examined to clarify the effects of the counter measure structure. The results indicate that the implementation of masonry blocks and the reinforcement installed behind them greatly improve the stability of the slope of the embankment, suppress the shear failure of the upper part of the embankment, and effectively prevent overall deformation of the embankment.

Keywords: small reservoir, centrifugal model experiments, dynamic response analysis, reinforced earthwork, seismic response

---

[1]PhD., Agr., Research & Development Institute, Takenaka Corporation, 5-1, 1-chome, Otsuka, Inzai-shi, Chiba, Japan, e-mail: wang.bohan@takenaka.co.jp, ORCID: 0009-0004-1253-2503
[2]Prof., PhD., Agr., Ibaraki University, 3-21-1, Amimachi chuou, Inashiki, Ibaraki, Japan, e-mail: yoshiyuki.mohri.office@vc.ibaraki.ac.jp, ORCID: 0009-0000-9180-2946
[3]Ms., Institute of Rural Engineering, 2-1-6 Kannondai, Tsukuba, Ibaraki, Japan, e-mail: tagataga@affrc.go.jp, ORCID: 0009-0005-2370-0231
[4]PhD., Agr., Institute of Rural Engineering, 2-1-6 Kannondai, Tsukuba, Ibaraki, Japan, e-mail: izumia309@naro.affrc.go.jp, ORCID: 0009-0008-5119-1659
[5]Prof., PhD., Agr., University of Tokyo, 7-3-1, Hongo, Bunkyo,Tokyo, Japan, e-mail: tad.tanaka@gmail.com, ORCID: 0009-0002-3296-5176

1. Introduction

There are about 100,000 small earthen reservoirs used for agricultural purposes in Japan, which were constructed more than 300 years ago using empirical methods. Many of these reservoirs require renovations due to the ageing of their embankments. The 2011 Pacific Coast Earthquake in East Japan resulted in extensive damage, including the loss of numerous lives due to the collapse of the reservoirs. The Ministry of Agriculture, Forestry, and Fisheries (MAFF) in Japan revealed that roughly over 2,000 reservoirs across the nation lacked adequate earthquake resistance [1]. Reinforcing these aged reservoirs against level 2 earthquake motion has become an urgent matter.

Elucidating the earthquake behavior of aged earth dam subjected to strong earthquake motions with observations and numerical predictions, furthermore, studying the deformation and collapse mechanism, seismic response of dam embankment are extremely significant for the mitigation and the assessment of the seismic safety of existing aged dam.

To implement seismic reinforcement of a vast number of small, ageing dams, it is important to be able to implement counter measures economically in the short term. Therefore, the reinforced soil method, which has been proven to be highly effective in reinforcing the foundation ground and soil structures, is one of the most effective counter measures for reinforcing existing reservoirs. In particularly, if it is demonstrated that high safety can be ensured by reconstructing a local portion of the embankment using the reinforced soil method, it can be applied to many existing reservoirs with simple construction [2].

In this study, centrifuge model tests were conducted to verify the seismic behavior of an embankment whose downstream portion was constructed by the reinforced soil construction method. In addition, elasto-plastic dynamic failure analysis is conducted to compare the results with those of the embankment deformation, settlement and dynamic response of the embankment.

2. Overview of reinforcement method

2.1. Reinforcement method for aged reservoir embankment

Most of the existing ageing reservoirs were constructed more than 300 years ago, and their structures are close to homogeneous and the degree of compaction is considerably lower than that of dams with modern construction techniques. No clear standards have been developed for construction methods to improve the seismic performance of such aged reservoirs. On the other hand, it is common for reservoirs damaged by earthquakes to have most of their embankments reconstructed, but the construction period is long and its cost is high. The 18.5-meter-high Fujinuma Reservoir, which collapsed by the 2011 Great East Japan Earthquake, had to be reconstructed according to new standards because most of the embankment had collapsed. It took ten years from the investigation of the cause of its failure to the completion of dam. Many of the existing reservoirs that have been judged to be in need of urgent seismic countermeasures due to insufficient seismic resistance are relatively small structures with an

embankment height of 10 m or less. Therefore, depending on the response characteristics of the embankment during an earthquake, it may be possible to improve safety by reinforcing a local portion of the embankment instead of reconstructing the entire embankment. Reinforced soil walls, which have been widely used in geotechnical engineering, have been researched and developed for the construction of steep slope embankments, and numerous field tests have revealed that the strength and deformation performance of slope works affect the stability of reinforced embankments [3, 4]. Furthermore, it has been shown that the safety of reinforced soil walls can be improved by connecting the reinforcing material of the embankment to the slope surface panels, blocks, or other slope works, because the effect of restraining the slope is improved [4]. The high safety of reinforced earth walls based on this method has been revealed, even though they were directly hit by the 1995 Hyogoken-Nanbu Earthquake, without significant deformation [5]. Although this method of reinforced earthwork has been applied to several large dams, it has not been widely used as a seismic countermeasure work for ageing reservoirs, and has been adopted only on a trial basis.

Liu et al. [6] conducted model tests at 1G field acceleration on rock-fill dams. They proposed various reinforcement techniques for these dams, including reinforcing the upper portion with geogrid and using stone blocks to protect the downstream slope surface. However, the reinforcement methods proposed by Liu et al. were investigated separately for the characteristics of geogrid and stone blocks, and the reinforcement effects resulting from combining these characteristics have not been validated. In this study, a simple reinforcing method for reservoir embankments was adopted by installing a short reinforcing material in the embankment at the slope end and constructing the slope works with concrete blocks, based on a reinforced earth wall structure that employs relatively short reinforcing material and slope construction [7]. This method is characterized by its ability to adjust the length of reinforcement material and the height of block walls according to the size and safety of the reservoir embankment, and to construct it at low cost and in a short period of time.

The proposed method for reinforcing the embankment involves enhancing the earthquake resistance of the entire structure by constructing an anti-soil pressure structure that integrates geogrid and masonry blocks within the embankment. The anti-soil pressure structure is located on the downstream slope side, where it can be easily constructed and can effectively reduce the shear deformation of the entire reservoir embankment, thereby improving its safety during earthquakes.

3. Reinforcement methods and experiments

To investigate the effectiveness of construction method to reinforce only a part of embankment for the age reservoir, a seismic model experiment was conducted on a medium-sized embankment with a height of approximately 9 meters.

The various measuring instruments such as accelerometers, laser displacement transducers, and a high-speed CCD camera were utilized to monitor the embankment's behaviors. The embankment structure used in the experiment was homogeneous type and was not reinforced in one case and reinforced by an anti-soil pressure structure integrating geogrid and masonry

blocks in another. Fig. 1 illustrates a schematic diagram of the masonry block reinforced model case. The height of embankment model was 30 cm and the depth of the foundation was 4 cm. The centrifugal force in the experiment was set to 30 G, so the height of the model corresponded to a dam height of 9 m when converted to a 1 G field. As shown in Fig. 2, the reinforcing section consists of five tiers of 2-cm-high blocks, with a reinforcing net connected to the back of the blocks, and the net embedded in the toe of the embankment. The reinforcement was made of plastic netting, which was sufficiently strong and did not break during the experiments. Table 1 shows the experimental conditions.
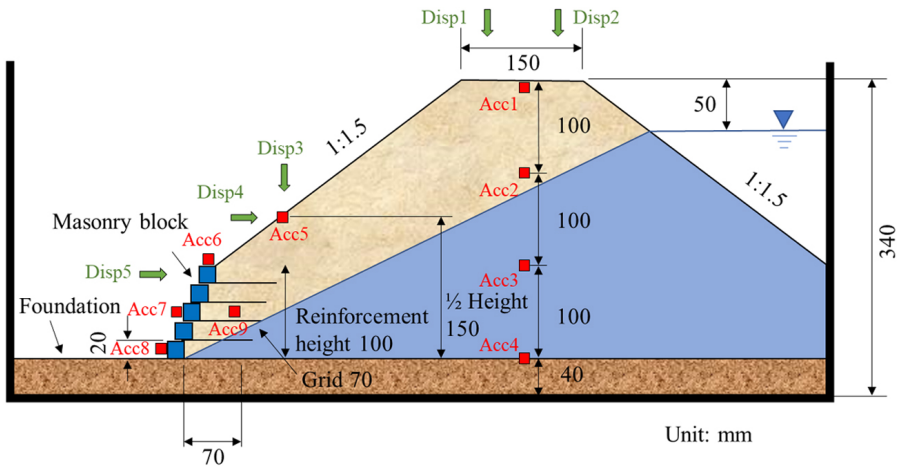
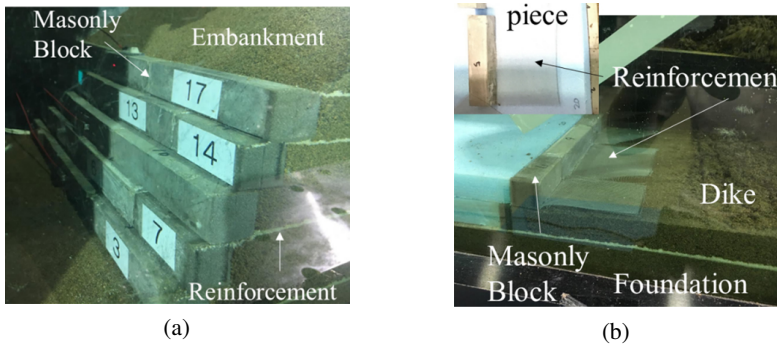Fig. 1. Cross section of experimental model

(a)   (b)

Fig. 2. Reinforced work (a), Arrangement of composite structure (b)

Table 1. List of experimental cases

Test Case	Density (Dc)	Reinforcement	Storage of water
CASE A	85%	×	○
CASE B	85%	○	○

In the centrifugal experiment, it is common to obtain the acceleration and deformation of the actual facility from the experimental results based on the law of similarity [8] shown in Table 2. At this time, as a condition for the scaled-down centrifugal experiment model of the original embankment, it is necessary to match the strength, deformation coefficient, permeability, etc. of the soil used with the characteristics of the actual embankment soil in the centrifugal field. However, since the particle size and its distribution cannot be adjusted to match the mechanical properties of the soil, general sand and silty soils has been commonly used in the centrifugal experiments of soil embankment. Therefore, in this research, the main purpose of this experiment was to understand the basic dynamic response of reservoir structures during an earthquake and to elucidate the effect of counter measure work.

Table 2. The law of similarity (N: centrifugal acceleration (G))

| | Density | Dimensions | Displacement | Velocity | Acceleration | |
					Centrifugal	Vibration
Prototype	1	1	1	1	1	1
Model	1	$1/N$	$1/N$	1	N	N
	Mass	Force	Stress	Strain	Time	
					Dynamic	Permeation
Prototype	1	1	1	1	1	1
Model	$1/N^3$	$1/N^3$	1	1	$1/N$	$1/N^3$

The foundation ground was constructed using Sawara silty sand with an optimum water content, density ratio of 95% D-value, and the embankment was constructed using Sawara silty sand with an optimum water content and density ratio of 85% D-value to simulate a typical aged reservoir embankment. Fig. 3 and 4 show the compaction curve and the particle size distribution of its sand. It has a fine fraction content of 13% and a maximum dry density of 1.723 g/cm^3, with an optimum water content of 15.42%. Physical properties of the materials are shown in Table 3. Metolose solution was used for storage water, and its concentration was adjusted to maintain the viscosity at 30 G equivalent to that of water at 1 G. The upstream water level was maintained at a height of 0.5 meters below the crest of the embankment, and shaking experiments were conducted after confirming the stability of seepage flow.

Table 3. Physical Properties of Sawara Sand

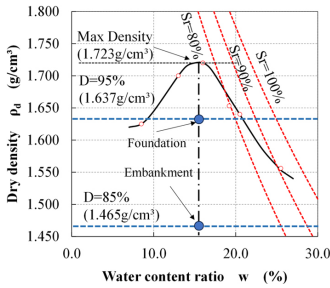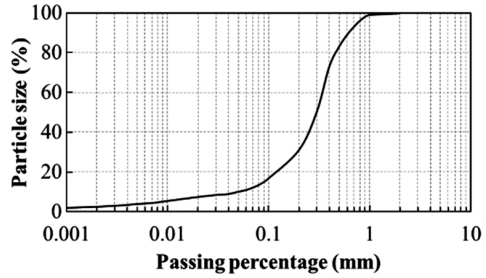| Item	Unit	Value
Soil particle density	g/cm^3	2.755
Maximum dry density	g/cm^3	1.723
Optimum moisture content ratio	%	15.42
Maximum particle diameter	mm	2.00
Fine fraction content	%	13

Fig. 3. Compaction curve

Fig. 4. Particle size distribution

As shown in Fig. 5, the vibration conditions are 20 waves of 3 Hz sinusoidal waves and multi-stage excitation with a maximum acceleration of 400 gal, with each stage increasing by 50 gal. This seismic waveform was converted to a 30 G field and used as the input seismic waves for the centrifuge shaking experiment. For clarity, the accelerations and deformations obtained from the experiment were converted to 1G field when organizing the data.
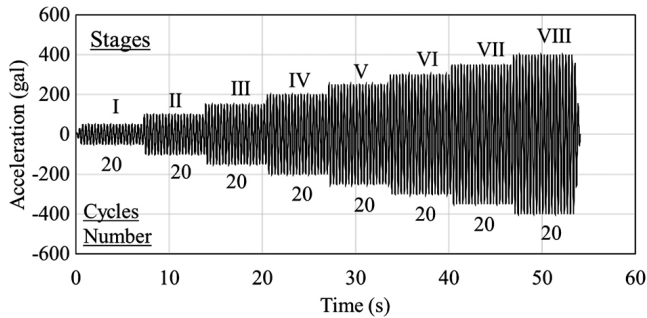

Fig. 5. Input waveform converted to 1 G field

3.1. Experimental model after the end of the excitation

Figure 6a and 6b present cross-sectional views of the entire embankment shape under seismic excitations of CASE A and CASE B, respectively, which have been converted to a 1 G field. The average settlement of the embankment was calculated as the mean of the measured settlements at the center of the crest and at a distance of 1.5 meters upstream and downstream of its surface. Remarkably, the average settlement of the crest in CASE B was 0.514 meters, indicating a 60% reduction in comparison to CASE A which the average settlement was 1.325 meters. These results provide evidence that local reinforcement of the downstream toe end of the embankment can control the overall deformation of the embankment behavior.

Figure 7 and 8 present the embankment damage following the seismic activity. In CASE A, the embankment caused two major slides, both of which reached the foundation ground at the toe end of the downstream slope. Conversely, in CASE B, where the embankment was

reinforced, the slip failure was constrained to the upper part of reinforced area and did not extend to the lowest part of the embankment. Furthermore, there was no discernible evidence of significant cracking at its crest, which has developed from the crest to the toe end.
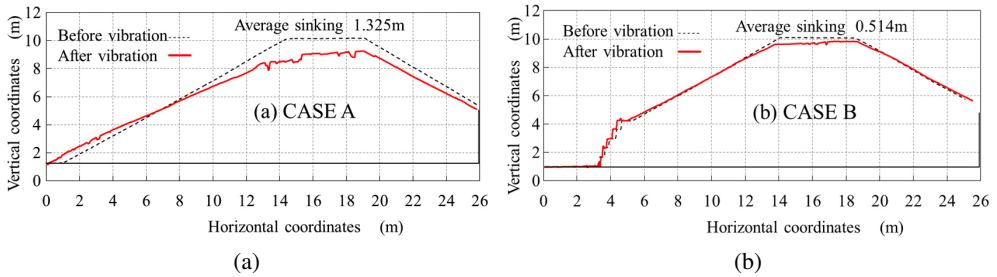

(a)

(b)
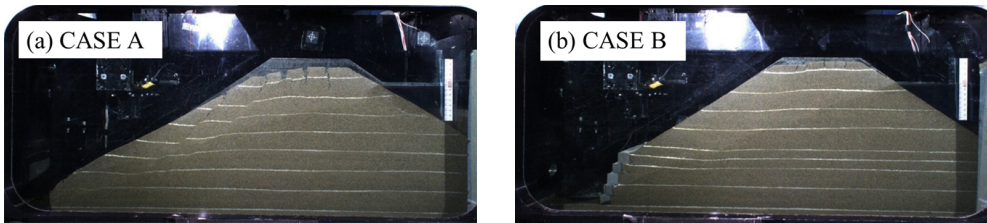
Fig. 6. Cross-sectional views by survey after excitation
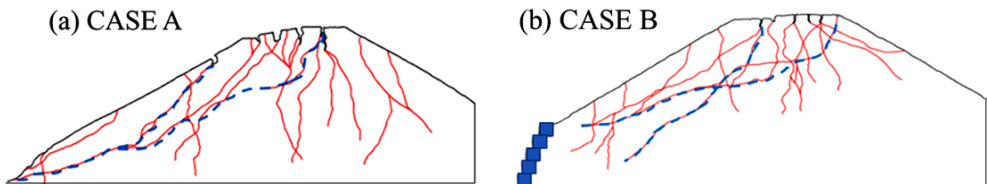

Fig. 7. Photograph of the body of the dam after excitation

Fig. 8. Sketch of the body of the dam after excitation (blue: continuous relatively large slip)

3.2. Behavior of the reinforce area

Figure 9 shows the horizontal displacement of the uppermost masonry block in the reinforced CASE B, while in unreinforced CASE A, the downstream slope surface at the same height as the uppermost masonry block, during each stage of input excitation. Notably, significant deformation was observed after 200-gal excitation in all cases. Moreover, the horizontal displacement of the blocks in the reinforced CASE B was found to be less than half of that observed in the unreinforced CASE A. This observation suggests that the block and reinforced sections effectively restrain the overall behavior of the embankment and increase its stability. Furthermore, Fig. 10 presents the amplification ratio of acceleration of the block wall

at each input excitation stage. Amplification is defined as the ratio of the measured maximum vibration at each point to the input vibration. It is clear evidence that the amplification ratio is more pronounced at the crest, and the overall magnification ranges from 0.8 to 2.5 times. Until the 200-gal excitation stage, the response of the block wall exhibited a decreasing trend with increasing input excitation. However, after the 200-gal stage, the response magnification slightly increased.
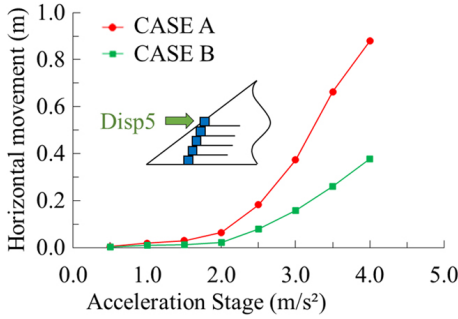

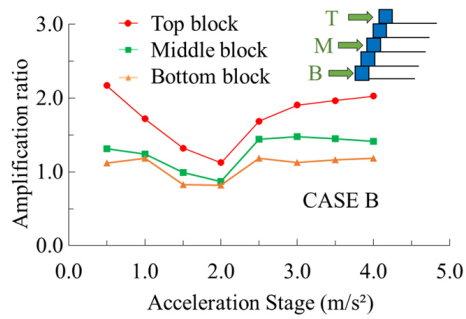Fig. 9. Horizontal displacement of slop surface

Fig. 10. Amplification ratio of acceleration for each block

3.3. Relationship between input acceleration stage and maximum response acceleration

The findings of the study reveal a correlation between the height of the embankment from the foundation and the response acceleration. Specifically, Fig. 11 shows the amplification ratio of acceleration of the embankment for each input excitation stage on the centerline of the embankment cross-section for CASE A and CASE B. It is observed that the response magnitudes at all locations except the crest are substantial when the input excitation is small, while the response magnification decreases as the input excitation increases. This phenomenon can be attributed to the expansion of the damaged region inside the embankment. In addition, it is revealed that the area of damage inside the embankment was reduced by the reinforcement of the slope, as shown by the photographs and cross-sectional sketches after the experiment.

Figure 12 shows the relationship between the height from the foundation (on the embankment centerline) and the response acceleration on the centerline of the embankment cross-section for each input excitation stage for CASE A and CASE B. In CASE A (unreinforced), the values of the maximum acceleration are higher at the upper part of the embankment for stages up to 200 gal of input excitation. However, when the input excitation exceeds 200 gal, the maximum response acceleration at 6 meters above the foundation clearly decreases, indicating that significant shear failure occurred to the embankment in the area from 3 meters to 6 meters above the foundation. Moreover, when the input excitation is 250 gal, the response acceleration of the crest is maximum, and the acceleration exceeds 1500 gal, with the amplification ratio of 6–7. In contrast, when the input excitation is 350 gal, the response acceleration of the crest
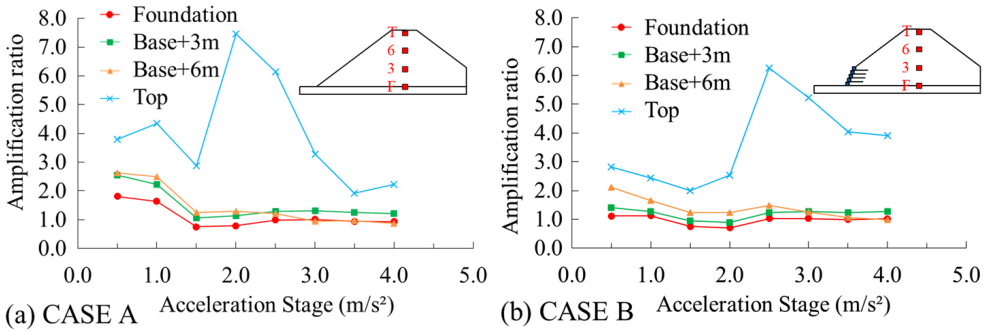
Fig. 11. Relationship between dam height and the amplification ratio of acceleration of embankment

is 700 gal, with the amplification ratio is 2. So its amplification ratio at the crest decreased than that at 250 gal excitation. In CASE B (reinforced), the maximum acceleration values are higher in the upper part of the embankment at stages up to an input excitation of 250 gal. Furthermore, the response acceleration at the position 6 meters above the foundation decreases from the input excitation of 300 gal. However, when the input excitation is 400 gal, the response acceleration at the crest is 1600 gal, with the amplification ratio of 4.0. It is clear that the response acceleration in the embankment is amplified from the foundation to the crest, but it shows complex behavior affected by the soil failure and deformation of the embankment. In particular, when the unreinforced embankment is subjected to large deformation or the failure zone expands, the response at the crest is greatly attenuated. Conversely, in the case of reinforced embankments, the response of the crest is not significantly attenuated.
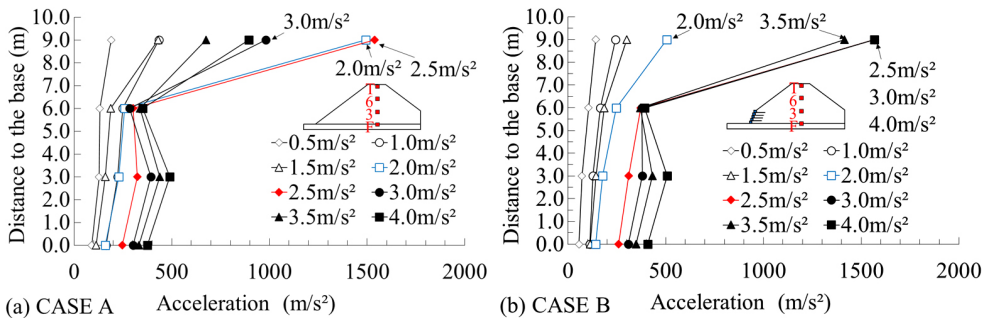

Fig. 12. Variation of maximum acceleration with dam height per acceleration stage

3.4. Relationship between excitation and embankment deformation

Figure 13 presents a graphic representation of the maximum settlement observed at the crest following each input excitation stage, which was converted to a 1 G field. Notably, settlement of the crest became perceptible once the input excitation stage reached 150 gal. Moreover,

the acceleration-settlement curve exhibited a steeper slope at the 150-gal stage, which could indicate the occurrence of damage or slippage in the embankment. Furthermore, the settlement observed at the crest of the reinforced embankment was generally lower than that of the unreinforced embankment. A maximum settlement of 0.7 m for CASE A corresponded to 8% of the embankment height, while in CASE B, maximum settlement of 0.2 m was 2% as the same way. Difference between the results of the two experiments was 0.45 meters at an input excitation of 400 gal. Figure 14 shows the settlement and the horizontal displacement of the mid-height slope surface position of the embankment. As with the crest, the deformation of this location increased from the 150-gal stage of input excitation. Upon comparing the horizontal displacement, it was observed that the horizontal displacement of the entire embankment was lower in the reinforced case than in the unreinforced case. This finding suggests that proposed reinforced embankment resist the seismic deformation of the embankment, significantly mitigating the occurrence of major cracks and settlements that penetrate deeply from the crest.
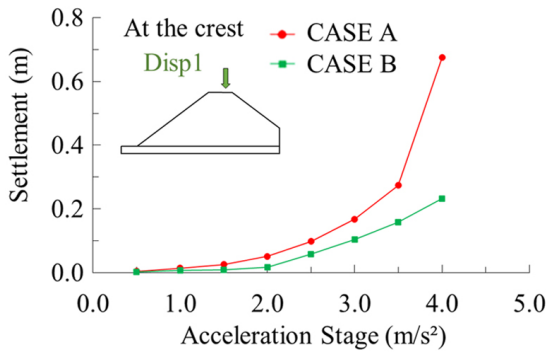
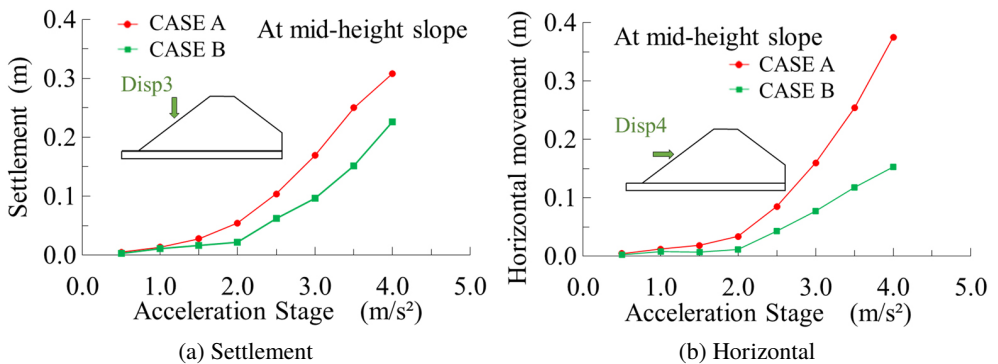Fig. 13. Relationship between the settlement at the crest and input excitation stage

(a) Settlement

(b) Horizontal

Fig. 14. Relationship between the settlement at mid-height slope position and input excitation stage

4. Comparison of experimental and analytical results on the behavior of embankment

4.1. Material model for the behavior of geomaterials

To investigate the seismic settlement, acceleration response, and strain generation of the embankment under centrifuge shaking experiments, two-dimensional Finite Element Method (FEM) analyses were executed for two cases of saturated embankments, designated as CASE A and CASE B. In previous studies, regarding the numerical analysis of seismic behavior of dams composed of soil, Wu et al. [9] conducted replication tests of centrifuge loading on dams using the LIQCA software. LIQCA is an elastoplastic dynamic analysis tool capable of solving soil skeleton accelerations and excess pore water pressure simultaneously, requiring precise consideration of the interaction between soil and water within the actual dam. This paper compares the results of the centrifugal shaking experiment of the rockfill dam with the analysis results, and mentions the predictive ability of the analysis.

In this study, we utilized Nonsolan, a full-stress dynamic response analysis code proposed by Prof. T. Tanaka [10], which could predict soil failure. This code adopts an elasto-plastic model that accurately predicts the peak strength and strain softening behavior of soil. The soil yield function in the analysis was modeled using the Mohr–Coulomb type, while the plastic potential was modeled by the Drucker–Prager type.

A material model for a real granular material is used with the features of nonlinear pre-peak, pressure-sensitivity of the deformation, strength characteristics, non-associated flow characteristics, post-peak strain softening and strain-localization into a shear band with a specific width. The yield function (f) and the plastic potential function (Φ) are given by

$$(4.1) \qquad f = \frac{2 \sin \phi}{\sqrt{3}\,(3 - \sin \phi)} I_1 + \frac{\sqrt{J_2}}{g\,(\theta_L)} - \frac{6c \cos \phi}{\sqrt{3}\,(3 - \sin \phi)} = 0$$

$$(4.2) \qquad \Phi = \frac{2 \sin \psi}{\sqrt{3}\,(3 - \sin \psi)} I_1 + \sqrt{J_2} = 0$$

where I_1 is the first invariant (positive in tension) of deviatoric stress and J_2 is the second invariant of deviatoric stress. With the Mohr–Coulomb model, $g\,(\theta_L)$ in Eq. (4.1) takes the following form.

$$(4.3) \qquad g\,(\theta_L) = \frac{3 - sin\phi}{2\sqrt{3} \cos \theta_L - 2 \sin \theta_L \sin \phi}$$

where ϕ is a mobilized friction angle and θ_L is the Lode angle.

The introduction of shear banding in the numerical analysis was achieved by introducing a strain localization parameter s in the following additive decomposition of total strain increment as follows.

$$(4.4) \qquad d\varepsilon_{ij} = d\varepsilon_{ij}^e + sd\varepsilon_{ij}^p, \quad S = \frac{F_b}{F_e}$$

where F_b is the area of a single shear band in each element, and F_e is the area of an element.

An one-point integration method and an hourglass control scheme are used with 4-noded two dimensional isoparametric element [11]. This element is effective and suited for collapse analysis of frictional material with shear banding. The most fully integrated continuum elements tend to lock especially for geomaterials, so the selection of element type is important for the collapse analyses of embankment dams. Simple shear strength is appropriate for earthquake response analysis of a fill-type dam and triaxial test results of layered soil sample are approximately equivalent to shear strength of horizontally anisotropic fill materials. We employed the triaxial test results for the two-dimentional dynamic analyses of fill-type dams.

4.2. Analysis of embankment soil

The excitation input in the centrifuge field was applied to the model under the initial stress conditions to acquire the embankment's behavior during an earthquake.

The finite element mesh of the centrifuge experimental model and the parameters used in the analysis are presented in Fig. 15 and Table 4, respectively. The unreinforced model was constructed with 1549 nodes and 1519 elements, whereas the reinforced model had 1255 nodes and 1225 elements. A thin layer of finite elements was placed between the inter-stacked blocks to account for frictional resistance, and the netting of the reinforcement was represented by truss elements. The boundary conditions were fixed in the *XY* direction at the bottom line and in the *X* direction on both side ends.
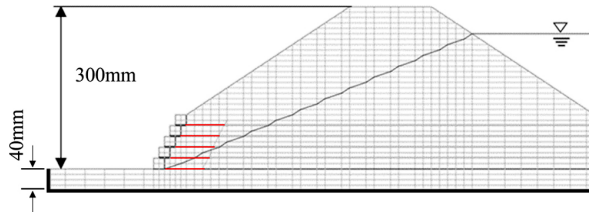

Fig. 15. Finite element mesh for dam (Dam mesh of reinforced case)

Table 4. Analytical parameters

Material	E (kg/cm^2)	v	ρ (kg/cm^3)	φ (deg)	c (kg/cm^2)
Saturation of foundation	300	0.3	0.0202	24	2.7
Saturated body of the dam	300	0.3	0.00192	22	0.12
Unsaturated body of the dam	300	0.3	0.00168	35	0.08
Block	210000	0.25	0.00225	–	–
Grid	7200	0.45	0.0001	–	–

To get the embankment model's strength, Sawara sand samples were prepared with a compaction degree D value of 85% same with the experiment. Subsequently, undrained triaxial compression tests were conducted after isotropic consolidation. The results indicated that the total stress strength comprised an internal friction angle φ_{cu} of 15.7° and a cohesion

C_{cu} of 4.1 kPa. Moreover, the effective stress strength comprised an internal friction angle φ' of 28.5° and a cohesion C' of 2.0 kPa.

In the investigation of the embankment's soil strength, the specimens underwent isotropic consolidation, following which an analysis of the initial stress results revealed a coefficient of lateral soil pressure ($K = \sigma_h/\sigma_v$) of approximately 0.8 to 0.3 at various locations throughout the embankment. To determine the strength under anisotropic consolidation ($K = 0.8$), an anisotropic undrained triaxial compression test was employed. The simulated results of this test for anisotropic consolidation at $K = 0.8$ are presented in Fig. 16. The analytical findings provide a clear prediction of the peak strength. However, since the strength of all materials in the anisotropic state, including the unsaturated region, was not obtained, an estimation was made for the strength of the entire embankment region, with reference to the strength increase factor of the saturated embankment region where the test was conducted. The undrained strength was utilized for the area beneath the water table line, while the strength based on effective stress was utilized for the area above the water table line.
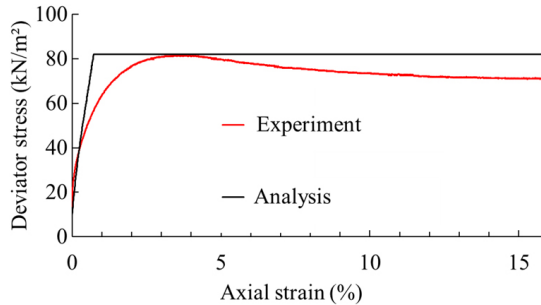

Fig. 16. Anisotropic consolidation triaxial compression test and simulation results

4.3. Dynamic respose analysis of centrifuge shaking experiment

The analytical and experimental results of horizontal displacement of the uppermost masonry block in CASE B (reinforcement) are presented in Fig. 17. Although the analysis predicted a final displacement 0.05 meters smaller than that observed in the experiment, the predicted time history response of the horizontal displacement corresponded well with the experimentally observed behavior. Fig. 18 illustrates the shear strain distributions from the unreinforced (CASE A) and reinforced (CASE B) analyses. Compared to the actual embankment failure shown in Fig. 8, the analysis predicts the shear failure of the embankment. In the unreinforced case, a clear slip surface was detected from below the crest of the embankment to the front of the downstream side slope, which tends to agree with the experimental results. In the case of reinforcement, no slip surface was detected up to the top of the reinforced area ahead of the slope, and it can be inferred that the large strain occurring within the reinforced area caused at the boundary between the reinforcing net and soil, rather than indicating a shear failure of the embankment. The reinforcement at the toe end of the downstream side slope prevented the development of shear strain throughout the embankment.
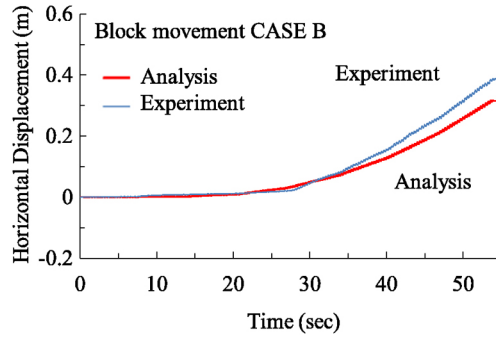
Fig. 17. Horizontal displacement of the uppermost masonry block (CASE B)
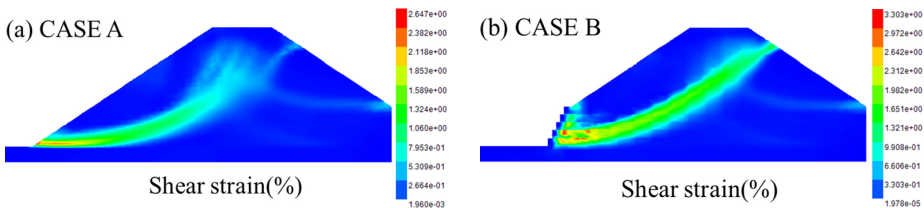

Fig. 18. Shear strain distribution

Response acceleration results for CASE A and CASE B are presented in Fig. 19 and 20, both experimentally and analytically. In CASE A, the analysis generally predicted the response acceleration of the crest, while in the large excitation, small disturbance at 6 meters above the foundation was not predicted. In CASE B, the response acceleration at the crest of the embankment demonstrated good predictability before the input excitation of 200 gal, but they cannot predict the observed responses to large input excitation of more than 250 gal. The behavior within the embankment at 6 meters above the foundation was similar to that of
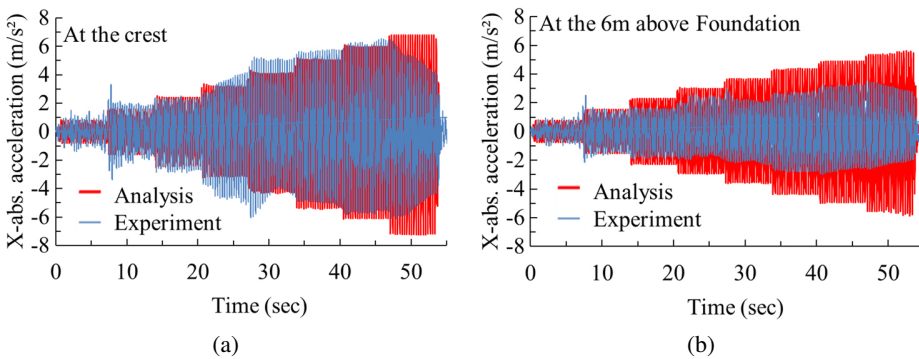

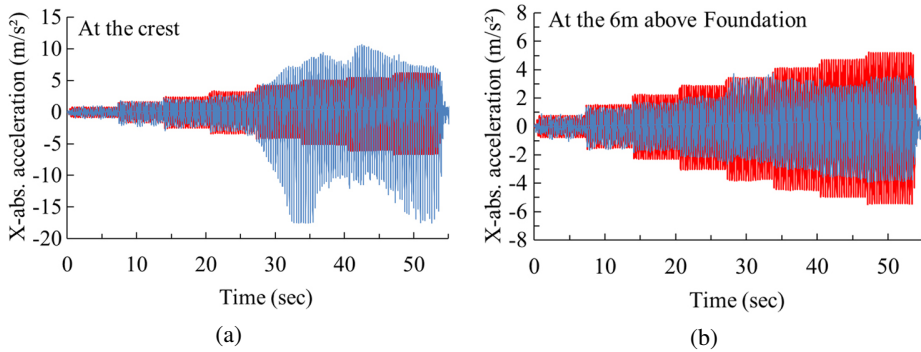Fig. 19. Acceleration response of the body of the dam (CASE A)

Fig. 20. Acceleration response of the body of the dam (CASE B)

CASE A, with irregularity observed at input excitation stages above 200 gal. Fig. 21 shows the settlement of the crest from the unreinforced (CASE A) and reinforced (CASE B) analyses and experiments. In the CASE A experiment, settlement began to occur after 10 to 20 seconds, whereas in the analysis, settlement began to occur after 20 seconds, which was a good prediction of the experimental results. In CASEB, the analysis predicted the experimental results well even better than CASE A. The analysis predicted the amount of settlement and the time of onset of settlement well.
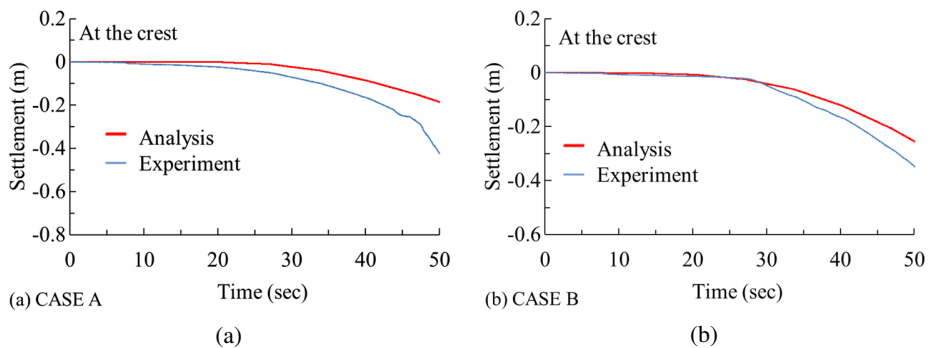

Fig. 21. Settlement of the dam (at the crest of the embankment)

5. Conclusions

This study aimed to investigate the feasibility of reinforcing the downstream embankment as a cost-effective approach for enhancing the durability of ageing reservoirs. The findings are presented below.

The partial reinforcement of the toe end of the embankment is effective in reducing the crest settlement to 40% and effectively prevent lateral deformation of the entire embankment.Elasoplastic FEM analysis which is capable of predicting the peak strength of soil, can predict the behavior of the embankment with slip failure in the unreinforced and reinforced cases.

References

[1] Ministry of Agriculture, "Forestry and Fisheries". [Online]. Available: https://www.maff.go.jp/j/nousin/bousai/bousai_saigai/b_tameike/. [Accessed: 27 April 2019].

[2] F. Tatsuoka, M. Tateyama, and J. Koseki, "Performance of soil retaining walls for railway embankments", *Soils and Foundations*, vol. 36, pp. 311–324, 1996, doi: 10.3208/sandf.36.Special_311.

[3] V. Gutierrez and F. Tatsuoka, "Role of facing in reinforcing cohesionless soil slopes by means of metal strips", in *Proceedings of the International Symposium on Theory and Practice of Earth Reinforcement*. 1988, pp. 289–294.

[4] M.B. Helwany, F. Tatsuoka, M. Tateyama, and K. Kojima, "Effects of facing rigidity on the performance of geosynthetic-reinforced soil retaining walls", *Soils and Foundations*, vol. 36, no. 1, pp. 27–38, 1996, doi: 10.3208/sandf.36.27.

[5] F. Tatsuoka, J. Koseki, and M. Tateyama, "Performance of reinforced soil structures during the 1995 Hyogo-ken Nanbu Earthquake", in *Earth Reinforcement – Proceedings of the International Symposium on Earth Reinforcement (IS Kyushu '96)*, vol. 2. Balkema, 1996, pp. 973–1008.

[6] J. Liu, F. Liu, X. Kong, and L. Yu, "Large-scale shaking table model tests of aseismic measures for concrete faced rock-fill dams", *Soil Dynamics and Earthquake Engineering*, vol. 61–62, pp. 152–163, 2014, doi: 10.1016/j.soildyn.2014.02.006.

[7] F. Tatsuoka, M. Tateyama, and O. Murata, "Earth retaining wall with a short geotextile and a rigid facing", in *Proceedings of the 12th International Conference on Soil Mechanics and Foundation Engineering (Rio De Janeiro)*. ISSMGE, 1989, pp. 1311–1314.

[8] R.F. Scott, "Summary of specialy Session 7- Modeling", in *Proceedings of Geotechnical Engineering Division Specialty Conference on Earthquake Engineering and Soil Dynamics*. ASCE, 1978, pp. 1417–1424.

[9] C. Wu, C. Ni, and H. Ko, "Seismic response of an earth dam: finite element coupling analysis and validation from centrifuge tests", *Journal of Rock Mechanics and Geotechnical Engineering*, vol. 1, no. 1, pp. 56–70, 2009, doi: 10.3724/SP.J.1235.2009.00056.

[10] T. Tanaka, "Elasto-plastic strain hardening-softning soil model with shear banding", in *Proceedings 15th ASCE Engineering Mechanics Conf. (CD-ROM)*. New York, 2002.

[11] D.P. Flanagan and T. Belytschko, "A uniform strain hexahedron and quadrilateral with orthogonal hourglass control", *International Journal for Numerical Methods in Engineering*, vol. 17, no. 5, pp. 679–706, 1981, doi: 10.1002/nme.1620170504.